Progress In Electromagnetics Research C, Vol. 130, 255–267, 2023

CSRR Based Metamaterial Inspired Sensor for Liquid Concentration Detection Using Machine Learning

Divya Prakash* **and Nisha Gupta**

Abstract—A sensor to accurately predict chemical concentrations has been proposed in this research work. Inspired by Metamaterials, the sensor is composed of Complementary Split-Ring Resonators (CSRRs) and utilizes the Machine Learning technique to accurately predict the concentrations. The sensor is designed to maximize the interaction of the Material Under Test (MUT) with the sensitive regions of the CSRRs. The usage of costly and complex fluidic channels and sample containers is avoided by using filter paper for the liquid MUT placement in between the resonators. The proposed sensor is small (2.3 cm × 2.3 cm), simple, employs a low-cost fabrication technique, and offers an alternate sensing mechanism that requires a minimal amount of the MUT. The multiple resonances exhibited by the proposed sensor add to the reliability and accuracy of the sensor.

1. INTRODUCTION

Metamaterials offer some unique attributes such as negative permittivity and permeability, backward wave propagation, negative refractive index, and these attributes are exploited in the design of perfect absorbers, filters, superlenses, cloaking devices, miniaturization, and performance enhancement in antennas [1–5]. The attractive features of the metamaterial-based sensors are their small size, low cost, ability to give instantaneous results, minimal sample requirement of the material under test (MUT), integrability with external electronic circuitry, etc. In the last few years, metamaterial-based sensors are designed for diverse applications in manufacturing, agriculture, health, food, and chemical industries. Examples of such applications are soil moisture sensor [6], blood glucose level sensor [7], early detection of cancerous tissues [8], adulteration detection in materials [9–12], detecting the quality of food grains [13], sensing concentration of liquids and characterization of materials based on their dielectric properties [14–19], etc.

In this work, we propose a sensor for the determination of liquid chemical concentration. Although several works have been carried out in the past to detect chemical concentrations, our proposed work is unique in the sense that the sensor structure is very simple facilitating easy placement of the liquid MUT in the proximity of the sensor. The placement of the liquid MUT around resonators to maximize sensitivity has been a design challenge that often requires fluidic channels and chambers to be separately designed and manufactured. This adds to the cost and complexity of the sensor. Broadside coupled Complementary Split Ring Resonators (BC-CSRRs) are used in the design to maximize the interaction of the MUT with the resonators for achieving high sensitivity [20–22]. The work also unitizes the Machine Learning (ML) concept to accurately predict the chemical concentrations from data obtained from the sensor. The proposed sensor is small, simple in design, and employs easy fabrication procedures using the low-cost photolithography technique. The sensing process is easy, offers instantaneous results, and requires a minimal amount of the sample to be tested. This sensing technique with some modifications

Received 1 November 2022, Accepted 23 February 2023, Scheduled 7 March 2023
* Corresponding author: Divya Prakash (divyabit18@yahoo.com).
The authors are with the Department of Electronics and Communication Engineering, Birla Institute of Technology, Mesra, Ranchi, Jharkhand 835215, India.

can also be used to test adulteration and the authenticity of liquid substances other than determining their concentrations. The shift in the resonant frequencies and changes in the magnitude of the reflection coefficient are the sensing parameters that are utilized to predict the chemical concentrations.

ML is now being increasingly utilized in applications accomplished through metamaterials. It is used to enhance targeted functionality, geometry optimizations, and forecasting performances [23–27]. A perspective on the ML-enabled computational sensors is presented in [23], and a new generation of compact and low-cost sensors with improved sensing capabilities is envisioned. In [24], a microwave sensor is proposed where a predictive model using ML is developed for the characterization of the Ethanol-Water mixture. Here, the ML model predicts the dielectric property of the mixture through the sensor's stopband centre frequency, using linear regression. In [25], a biosensor that utilizes ML for the sensor's behaviour prediction is proposed. Polynomial regression is used here to enhance the sensitivity using the most suitable sensor geometry. In [26], a metamaterial solar absorber is proposed, where ML is used to forecast absorption by examining the design data, considering the thickness of the metasurface and substrate, and angles of incidence. Our proposed work's novelty lies in the simple design with a cost-effective MUT placement mechanism along with the developed ML model that considers the multiband response of the sensor.

2. SENSING PRINCIPLE

Split ring resonators (SRRs) are commonly used in the design of metamaterial structures for various applications, and in our work, we have used a pair of complementary split-ring resonators (CSRRs). The placement of the MUT is done between the resonators. The resonating frequency of the resonator is decided by its geometry, the dielectric property of the substrate used, and the dielectric property of the material surrounding the resonator in proximity. Once fabricated, the dimensions of the structure cannot be changed. Hence, to bring about a shift in the resonating frequency, which is also the sensing parameter, the dielectric property of the material surrounding the resonator or the material itself must change. By changing the MUT itself, placed between the resonators, the resonant frequency of the design changes, giving an indication about the material. The general equation for the resonating frequency is given by Equation (1),

$$f_r = \frac{1}{2\pi\sqrt{L_u C_u}} \tag{1}$$

where C_u and L_u are the capacitance and inductance in the CSRR's equivalent tank circuit, without the MUT. The capacitance is developed from the split or gaps in the resonator rings, and as a result of the current flowing in the metal portion of the resonator, the inductance in the equation is created. The resonance frequency of the resonators with the MUT is given by Equation (2),

$$f_{rL} = \frac{1}{2\pi\sqrt{L_u(C_u + C_L)}} \tag{2}$$

where C_L arises as a result of the placement of the MUT in the proximity of the resonators, which changes the effective permittivity of the medium and hence the capacitance, which in turn changes the resonant frequency. The idea is to place the MUTs in regions of high electric field densities to maximize the sensitivity. There is a high concentration of electric fields in the etched rings of the CSRRs; therefore, the placement of the MUT around the etched rings would lead to high sensitivity of the sensor. The sensitivity and selectivity are the important attributes that decide the sensor performance. Multiband sensing is also a desirable attribute in sensor design, as it adds to the reliability and accuracy of the sensor [16, 19].

3. SENSOR DESIGN

The sensor comprises two CSRRs that are broadside coupled and face each other, as shown in Fig. 1. The split width in both the resonators is 1.2 mm. The dimension of the substrate on which the circular ring is etched is 23 mm × 23 mm. Rogers RO3003 is the substrate used, whose dielectric constant value is 3; the value of loss tangent is 0.001; and the substrate's height is 1.52 mm. The inner and outer radii

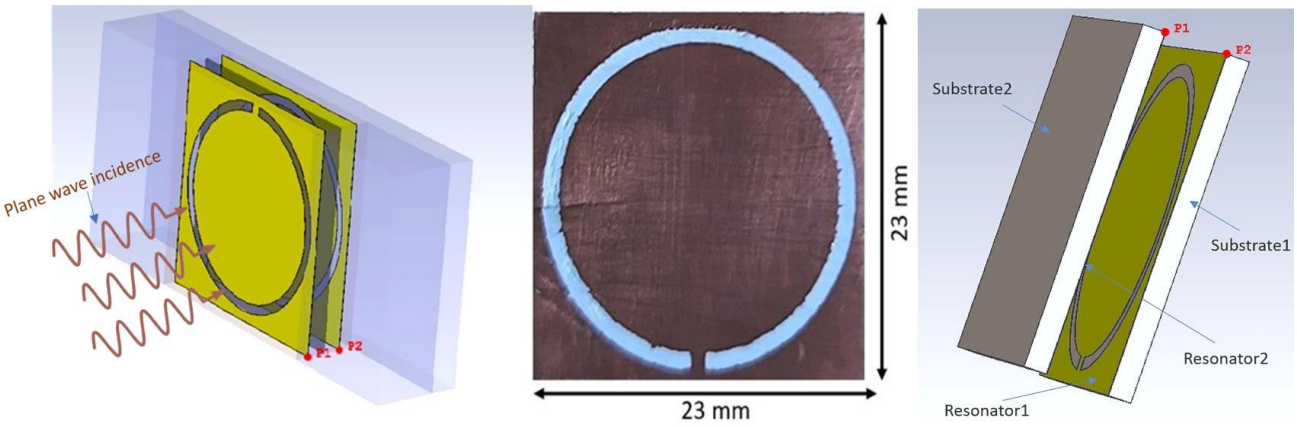

(a) (b) (c)

Figure 1. (a) Structure of the resonators placed within the sample holder with a plane wave incidence. (b) Fabricated resonator with dimensions. (c) Orientation of the resonators etched on the ground plane, as placed within the waveguide.

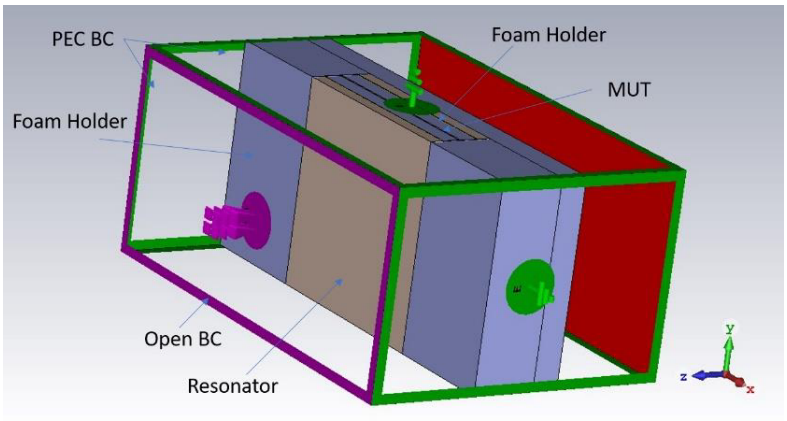

Figure 2. The sensor placed in the foam holder along with the boundary conditions applied in the simulation.

of the etched ring in both the resonators are 10.5 mm and 9.6 mm, respectively. P1 to P2 is the distance between the resonators. The simulations are carried out in the CST Microwave Studio software. As the sensor is intended to be tested in a waveguide, the perfect electric conductor boundary conditions are applied around the x- and y-axes, and the excitation signal travels along the z-axis, as shown in Fig. 2. Both the magnetic and electric fields lie on the resonator's plane. On one side of both the resonators, a circular ring is etched, and on the other side, the metal layer is completely removed through etching. The MUT is placed between the two resonators. At the resonant frequency, there is a high concentration of electric fields in the etched rings of the resonators, thus the placement of the MUT around the rings yields high sensitivity. The MUT is placed in the waveguide through a holder made of foam having a dielectric constant approximately that of the air. The dimensions of the resonators are small, and they are lightweight. Moreover, the amount of MUT required for sensing is miniscule. Therefore, the choice of foam as a sample holder is appropriate, and it would easily provide the mechanical strength needed to hold the resonators and the MUT. The intended waveguide to be used is that of C band, and the resonators along with the sample holder and the MUT easily fit into the waveguide's opening. As sensing is done in terms of the resonant frequency shifts, the geometry of the resonators (that decide the resonant frequency) is chosen so that they fit in the waveguide. Operating frequencies lying in the

C-Band gives optimum size of the resonators, i.e., the CSRR ring area is large enough for its sufficient interaction with the MUT to bring about greater shifts in the resonant frequency. Meanwhile, the resonators are also comparatively small to be fabricated and handled easily, having low cost.

For the liquid MUTs, filter paper is used in the design. The filter paper with added Liquid Under Test (LUT) on it [20] is placed on the foam layer between the resonators. The foam layers are added to keep a distance between the resonators and to provide a platform for the filter paper wetted by the LUT.

As discussed in [28], several methods have been adopted in research works for the placement of the LUTs around the resonators. In some works, containers are used to hold the LUTs. Although containers allow large sample volumes, their thick walls waste the sensitive metasurface, limiting the sensitivity of the sensor. Capillary tubes and microfluidic channels are also used for the placement of LUTs. The contact ability of the capillary tubes with a flat resonator surface is limited owing to its cylindrical shape. The design of microfluidic channels requires additional fabrication cost and setup. These techniques also require external mechanical systems to fill and empty the channels, like pumps and syringes. Filter paper wetted with the LUT is a low-cost and simple technique for the placement of samples in proximity to the resonators. The filter paper is very thin, and it can be easily exposed to the full sensing area where the fields are concentrated, with homogenous distribution of the LUT. Pipettes are used to drop the liquid samples over the filter paper easily, ignoring the use of any external mechanical supply system.

4. APPLICATIONS

4.1. Ethanol Concentration Sensing

After finalizing the application, the next step in the design process involves the simulation of the proposed sensor with the MUTs. Since it is intended to build a concentration sensor, for the simulation purpose it is required to know the dielectric properties of the Water-Ethanol solution at various concentrations. After preparing samples of different concentrations, using the dielectric probe kit, the dielectric constants of various concentrations of ethanol in water are measured. The dielectric constant of the Ethanol/Methanol-water solution at different concentrations is measured over a broad frequency range (1–12 GHz) and plotted in Fig. 3. The plot clearly shows the slope of the curve, i.e., the variation of the dielectric constant vs frequency. At the resonant frequencies, the slope of the curve gives an estimation of the changes in the dielectric constant values, which are eventually put in the simulation software. The values of the dielectric constants, Fig. 3, obtained from the probe kit are like those mentioned in [29, 30]. The values of the real part of the complex permittivity and the loss tangent obtained from the probe kit are fed into the simulation software (CST Microwave Studio) to obtain the reflection coefficients at different ethanol concentrations. The dielectric properties of the

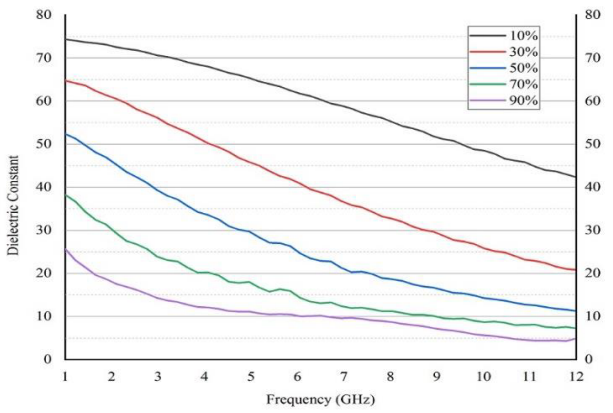

Figure 3. Plot of dielectric constant of Ethanol concentrations in the 1–12 GHz frequency range.

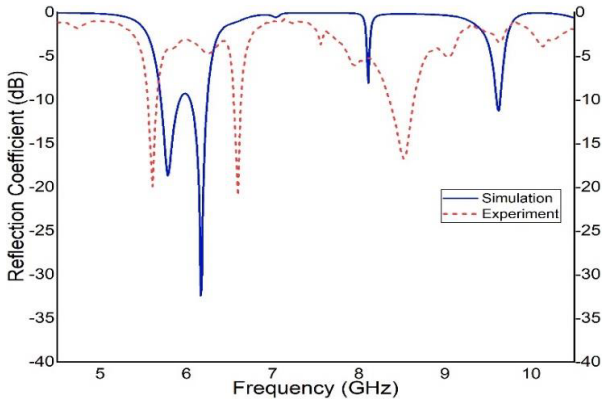

Figure 4. Experiment and simulation data comparison for dry filter paper as the MUT.

filter paper are also measured, which is found like those mentioned in [28]. First, a dry filter paper is placed between the resonators, and the reflection coefficients at different frequencies are obtained. Fig. 4 shows the comparison between the reflection coefficients obtained through the software simulation and the experiment. In the experiment, the dry filter paper is just placed between the resonators and the foam material as done in the simulations.

Both simulation and experimental data show three resonances between 5 GHz and 10 GHz. Out of the three resonant notches, two lower frequency notches are in proximity. The reflection coefficients for 10%, 20%, 30%, 40%, 50%, and 60% Ethanol concentration in water are plotted in Fig. 5.

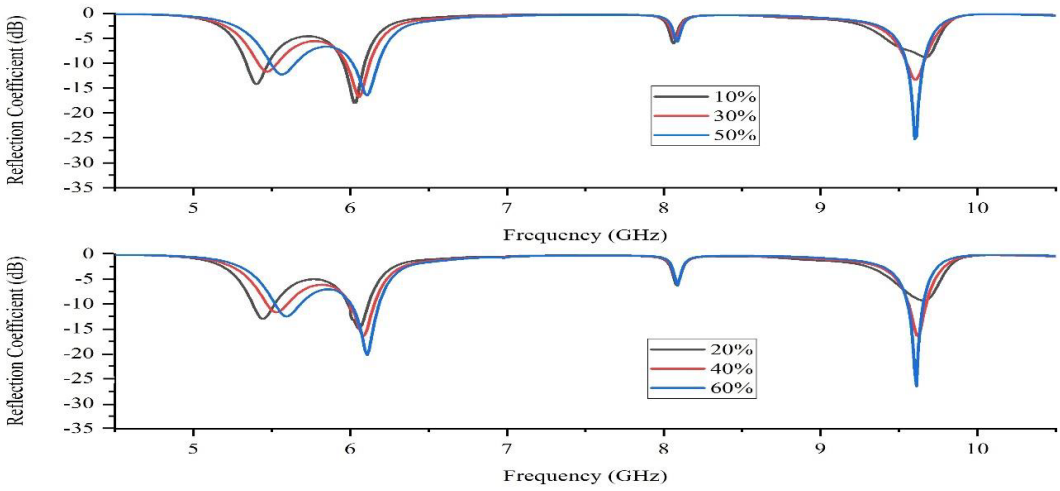

Figure 5. Reflection coefficient vs frequency plot for Ethanol as MUT at various concentrations.

There is a shift in the first two resonant frequencies as the concentration is increased from 10% to 60%, while the amplitude of the reflection coefficient decreases with the increase in the concentration at the third resonance. The linear shift in the first two resonances and the linear change in notch depth at the third resonance can uniquely identify the concentration of ethanol. In the experiment, three drops of the solution are dropped using a pipette at the centre of the filter paper which is placed between the resonators and the foam material. The whole setup, consisting of the resonators and the wetted filter paper on the foam holder, placed within a waveguide adaptor, is shown in Fig. 6. The setup

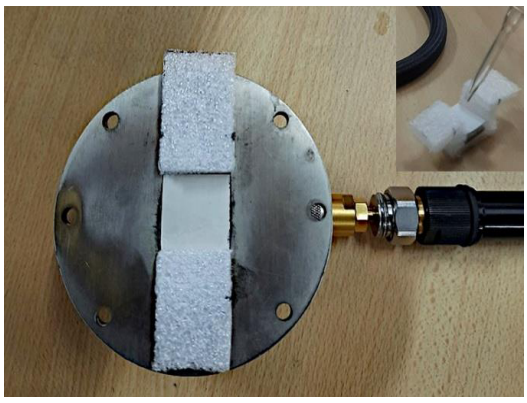

Figure 6. The wetting of the filter paper with the MUT and the placement of the resonators along with the MUT in a waveguide adaptor through a foam sample holder.

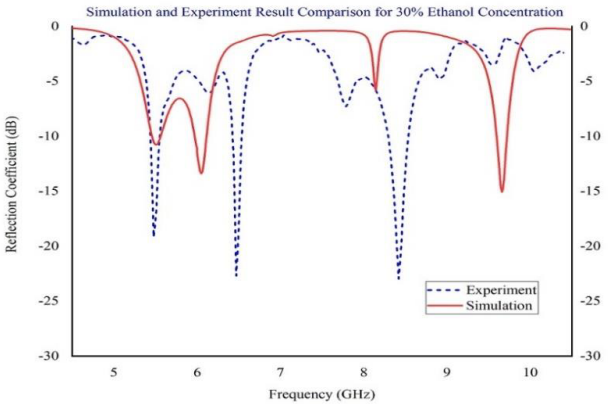

Figure 7. Reflection coefficient curves for 30% Ethanol concentration as obtained from the simulation and experiment.

is then excited by the Vector Network Analyzer (VNA) to get the reflection coefficients for varying concentrations. Fig. 7 illustrates the comparison of the reflection coefficient curves as obtained through the experiments and simulations, for 30% Ethanol concentration. The two curves are similar, each having three notches in the mentioned frequency band.

The difference in the frequencies of the notches and notch depths occur due to fabrication inaccuracy, inaccurate foam holder dimensions, inhomogeneous distribution of the liquid MUT over the filter paper, imprecise separation of the resonators through the foam material, calibration errors, and probe losses. Since the sensing parameter is the resonance frequency shifts and the changes in the notch depths, the differences in the notch frequencies as obtained through the simulation and experiment do not affect the sensor performance or the sensitivity, also discussed in [11].

4.2. Methanol Concentration Sensing

Figure 8 shows the dielectric constants of various concentrations of methanol-water solution in the frequency range of 1 GHz to 12 GHz, as obtained from the dielectric probe kit.

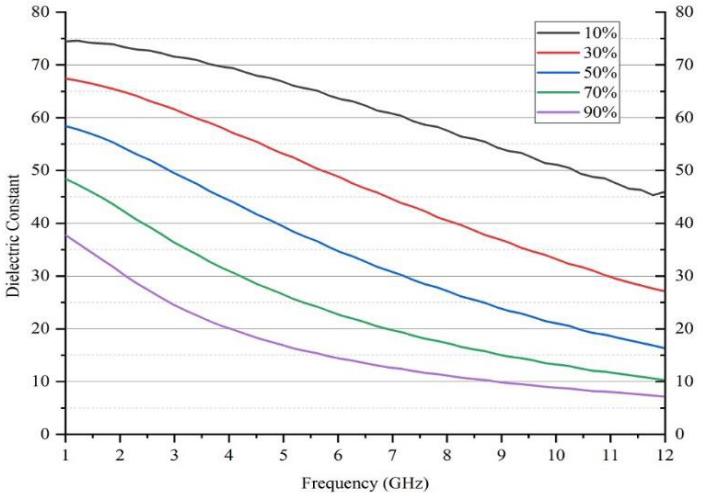

Figure 8. Plot of dielectric constant of Methanol concentrations in the 1–12 GHz frequency range.

Like the ethanol concentration sensing, in the experiment, three drops of methanol-water solution are dropped on the centre of the dry filter paper placed between the resonators and the foam material. This process is carried out for the 10%, 20%, 30%, 40%, 50%, and 60% Methanol water concentration. For each concentration, the resonant frequencies and notch depths were captured. Fig. 9 depicts the plot of the reflection coefficient vs frequency, obtained through simulation of the sensor with the data of dielectric properties of methanol-water solution. It is observed that the resonant frequency of the first notch shifts more than the second notch, and the amplitude of the third notch decreases with the concentration increments, with the notch frequency being almost the same.

Figure 10 depicts the contrast between the reflection coefficient curves as obtained through the experiment and simulation, for 30% Methanol concentration.

With accurate fabrication using precision instruments, the differences between the measured and simulated results could be eliminated. The foam holder's accurate shape and size are critical as inaccuracy would lead to a tilted orientation of the sensor within the waveguide adaptor. Moreover, any slight change in the separation between the resonators would lead to deviation from the simulated results. Care must be taken to ensure that the unvarying amount of MUT is dropped on the filter paper at the same location for every measurement. The VNA must be properly calibrated before taking any measurements. The measured results for the dry filter paper, concentration of Methanol, and Ethanol as the MUT show similar reflection coefficient responses to the simulation, with all three notches present around the same frequencies. Eliminating the mentioned sources of errors would lead to a perfect

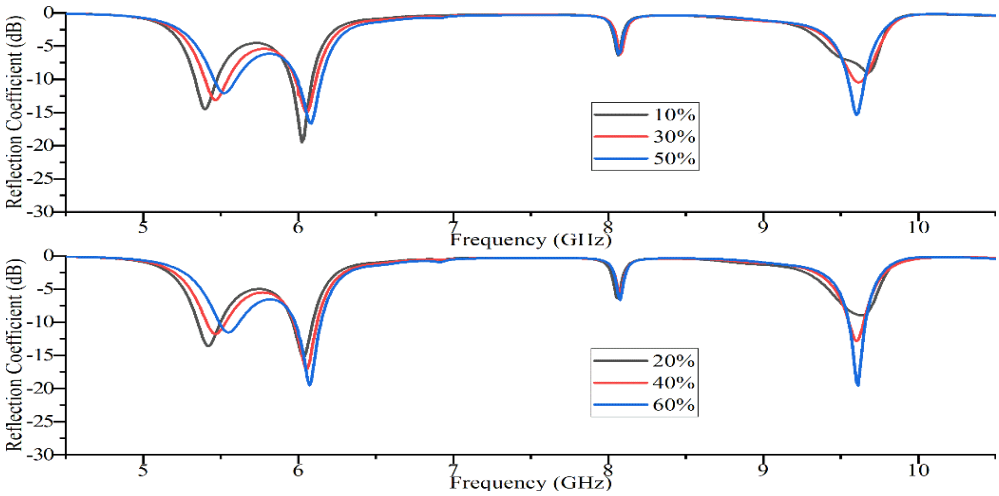

Figure 9. Reflection coefficient vs frequency plot for Methanol as MUT at various concentrations.

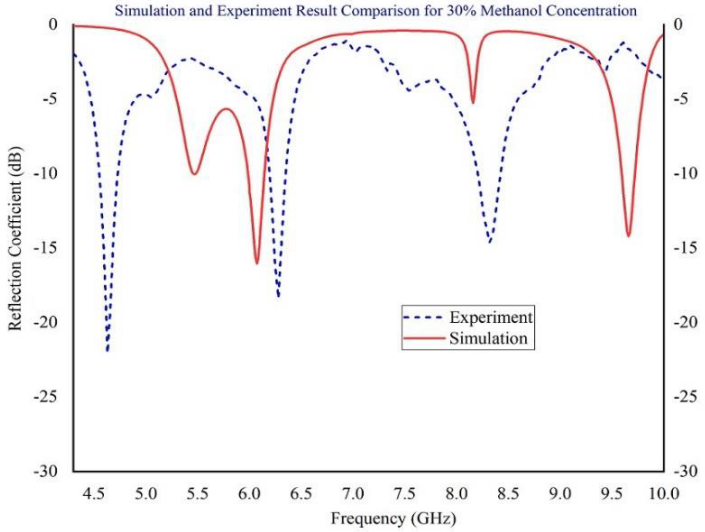

Figure 10. Reflection coefficient curves for 30% Methanol concentration as obtained from the simulation and experiment.

match between the experimental and simulated results. As mentioned, only the dielectric properties of ethanol/methanol solution are measured in the 1–12 GHz frequency range using a dielectric probe kit and VNA. Further, as shown in the simulation results, the sensor depicts resonance characteristics at three frequencies between 5 GHz and 10 GHz (one of which goes beyond 8 GHz); therefore, to verify it experimentally, a C-band through X-band waveguide to the co-axial adapter is used as shown in Fig. 6, whose passband goes up to 11 GHz.

5. PREDICTIVE MODEL GENERATION USING MACHINE LEARNING

Figure 11 shows the variation of the first and second resonant frequencies (RF1, RF2) and notch depth (ND3, at the third resonant frequency) for distinct concentrations of Ethanol and Methanol in water. It is apparent from the plot that as the concentrations of Ethanol and Methanol increase, the resonant frequencies (RF1, RF2) increase, and the notch depth (ND3) also increases. The independent variables,

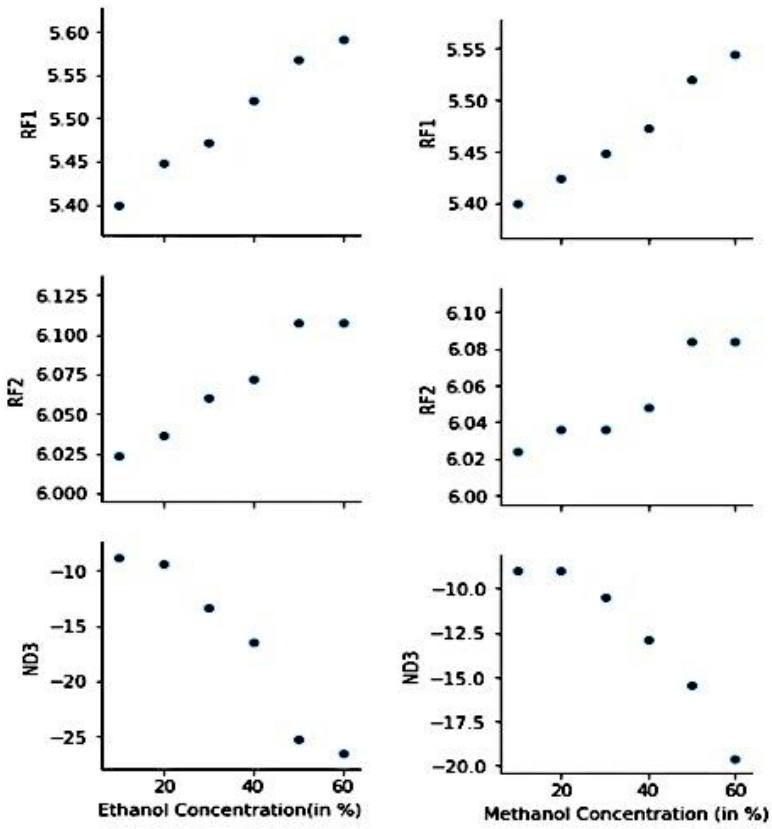

Figure 11. Plot showing the change of independent variables (ND3, RF2, RF1) with the variation of Ethanol and Methanol concentrations. RF1 and RF2 are in GHz, and the changes ND3 is measured in dB.

i.e., RF1, RF2, ND3, are unique for a particular concentration of either Ethanol or Methanol and thus could be used to build a model to predict the chemical concentration (dependent variable).

The data of these independent variables for each concentration of Ethanol and Methanol are tabulated, and using the Linear Regression function in Python programming language an equation to predict the concentration of each chemical in water is developed. The correlation values of Ethanol concentration to the RF1, RF2, and ND3 are found to be 0.995, 0.98, and −0.965, respectively. Similarly, the correlation values of Methanol concentration to the RF1, RF2, and ND3 are found to be 0.992161, 0.940256, and −0.955574, respectively. From Fig. 11 and the correlation values, it is apparent that the Ethanol and Methanol concentrations are linearly correlated to the independent variables. The tabulated data of Ethanol and Methanol concentrations and the corresponding independent variables are split into training and test data by using the 'Scikit-learn' library of the Python programming language and calling the 'train_test_split' function [31–33]. The training data are fitted to the Linear Regression function to obtain the regression coefficient and the y-axis intercept or the regression constant value. For the independent variables RF1, RF2, and ND3 (ethanol-water solution) the coefficients of regression are found to be 208.173615, −5.766147, and −0.024454, respectively. The y-axis intercept or the regression constant value is −1074.5. Similarly, for the Methanol solution, the regression coefficient values for RF1, RF2, and ND3 are −17.689832, −18.500106, and −4.477106, respectively. The intercept value is 191.156. The general equation for the concentration takes the form of (3),

$$C = k1 \cdot \mathrm{RF1} + k2 \cdot \mathrm{RF2} + k3 \cdot \mathrm{ND3} + Y \tag{3}$$

where C is the concentration in percentage; $k1, k2, k3$ are the coefficients of regression; and Y is the regression constant. Just by finding the independent variable values, through the excitation of the sensor with the MUT, the concentration can be known easily through the equation. The highest accuracy obtained from the model and the simulated data is found to be 94.55% for Ethanol water

solution and 94.85% for Methanol water solution. Thus, the predictive models for both Ethanol and Methanol solutions offer high accuracy.

In an application like ours, [24] proposes a microwave sensor, assisted by ML, for dielectric characterization of the Ethanol-Water mixture. A predictive model using ML is developed employing Linear Regression. As compared to our work, where the multi-band response is used to build the predictive model, [24] uses a single transmission notch frequency to build the model. Moreover, in comparison to our simple MUT placement mechanism using filter paper, it uses a 3D-printed liquid container placed in an empty region in the main sensing unit, which adds to the cost and complexity of the sensor design. In [25], a Graphene refractive index sensor based on a metasurface with increased sensitivity, assisted by Machine ML, for the detection of haemoglobin is proposed. To predict the absorption values for different sensor design parameters, an ML algorithm has been proposed. The absorption response of the sensor changes for different haemoglobin concentrations. Here, Polynomial Regression models are used to predict the best geometrical parameters to achieve high sensitivity. Selecting the algorithm that is best suited to build an accurate predictive model could be done with some prior knowledge of the sensor data as done in [34], where investigation of different concentrations of acetone/methanol mixtures in water is carried out, with added temperature compensation. As in our work, the independent variables are linearly correlated to the dependent variable, i.e., the unknown concentration, and the choice of using Linear Regression is easy. In [35], a CRLH-TL-based sensor having multiband resonance is proposed that uses ML to enhance the sensitivity to a specific MUT rather than the effective medium. The MUTs used here are different concentrations of Methanol, Ethanol in water. The multiband response is achieved through different lengths of the stub inductors. Unlike our simple MUT placement mechanism, a fluidic channel that runs over the interdigital capacitor (IDC) section is used to place the MUT. To enhance the sensitivity of detection, [36] uses unsupervised ML to analyze the transmission spectrum. Here, to detect the carbendazim concentrations, a metamaterial structure composed of a cut wire and two SRRs (CWSRRs) was used. In [37], to find the complex permittivity of the Water-Ethanol solution, a modified complementary electric-LC resonator (M-CELC) is proposed that consists of a central meandering slot and an etched pair of CSRRs for greater confinement of electric fields, thereby increasing sensitivity. Here the liquid MUT is injected through a syringe into a microfluidic channel made on a polydimethylsiloxane (PDMS) substrate placed above the meandering slot. Although this work achieves high sensitivity in comparison to our sensor design, it has a complex structure, and the microfluidic channel adds to sensor size and cost. Moreover, our proposed design does not require any fluid injection system using syringes. Conventionally, curve fitting functions are used to represent the sensor's response, but with the increase in the number of independent variables, the fitting function becomes complex and requires added computational power to build.

An accurate estimation of the output can also be made when the training data are taken from the measured values of the sensor. In this work, the regression model is developed from the simulation results, as they are valid and defensible, derived from globally accepted common rules and conditions. Although the simulation provides strict guidelines for the implementation of a design, the actual environment of operation of the device may differ. As a result, the measured values may contain noises and uncertainties arising from interference from the ambient environment (cross sensitivity [38]), fabrication anomalies, and material inconsistencies (purity of ethanol and methanol in this case). Thus, the measured values contain not only the information about the material being tested but also some information about the ambient environment and noises, and this information may be leveraged for precise calibration of the sensor. In [39], it is discussed how measurement uncertainty is used for estimating precise models for systems that have large experimental variations operating in noisy environments. While building a regression model from the measured values, care should be taken in choosing the independent variables. Although multi-variable regression can provide a better fitting model, choosing the independent variables that are highly correlated to each other or are redundant may lead to an overfitting model. As discussed in [38], a need may arise for recalibration in the final measuring environment, and in such instances, ML algorithms that optimize the regression models, minimizing the error between the predicted and actual values, may prove to be very convenient and time-saving. Table 1 elaborates on some of the metamaterial, sensor applications assisted by ML. In recent research works, the ML approach mainly employs Classification or Regression algorithms, or the combination of both, for targeted parameter enhancements and geometry optimizations.

Table 1. ML assisted metamaterial, sensor applications specifying ML approach, sensor topology, and sensing parameter.

Ref. No.	Application	Sensor Topology	ML Approach	Single/Multiband Sensing/Sensing Parameter
[35]	Characterization of Liquid Mixtures.	Zeroth-Order Resonator. Composite right-/left-handed transmission line (CRLH-TL).	Classification using Convolutional Neural Network (CNN).	Multiband. Shift in Resonance Frequency.
[25]	Haemoglobin Detection Biosensor.	Graphene-based metasurface.	Polynomial Regression for finding suitable geometrical parameter for sensitivity enhancement.	Change in Absorption of the metasurface.
[24]	Dielectric Characterization of Water-Ethanol mixture.	Transmission line with intercoupled spiral resonators.	Linear Regression	Single. Shift in transmission notch frequency.
[36]	Carbendazim Detection. Benzimidazole fungicide Detection.	Pair of Split-Ring Resonators and Cut Wire.	Mean Shift. Unsupervised Machine Learning.	Multiband. Shift in Resonance Frequency.
[34]	Investigation of different concentrations of Acetone/methanol mixtures in water with temperature compensation.	Split Ring Resonator with narrowed lower side, excited by a transmission line.	Classification followed by regression on the sensor's transmission profile data at different temperatures. High classification accuracy achieved through MLP, SVM, DT, LDA, KNN, and Random Forest.	Single. Shift in resonance frequency.
[40]	Plasmonic Biosensor for DNA detection.	Double Negative Metamaterial, thin film five layered structure.	MLP, AE, t-SNE, k-means clustering for enhanced sensor plasmonic structures and elevated detection sensitivity through geometry optimizations.	Single. Resonance shifts in reflectance curve.
This Work	Sensing Concentration of Ethanol/Methanol in water.	A pair of CSRRs excited in a waveguide.	Linear Regression.	Multiband. Shift in Resonance Frequency.

Abbreviations: *MLP: multilayer perceptron, SVM:support vector machine, DT: decision tree, LDA: linear discriminant analysis, KNN: K-nearest neighbors, AE: auto encoder, t-SNE: t-Stochastic Neighbor Embedding*

6. CONCLUSION

Metamaterial-based sensors offer an alternate sensing mechanism through the manipulation of electromagnetic waves. They are advantageous in the sense that they are small, low cost, employ an easy fabrication process using existing fabrication techniques, require a minimal amount of the material to be tested, and are even easy to integrate with external electronic circuitry. In this work, a metamaterial inspired sensor composed of a pair of CSRRs is proposed to detect chemical fluids. The sensor design is simple, and the placement of the liquid MUTs is accomplished with ease without

requiring any additional fluidic channels and containers, thereby reducing the cost and complexity of the sensor structure. A model is developed using machine learning, that predicts the chemical concentrations with high accuracy. The model's accuracy for sensing the concentration of Ethanol-Water solution was found to be 94.55%, and the accuracy for Methanol-Water solution was 94.85%. The sensor can also be used to sense the adulteration of liquid fuels and to check the authenticity of liquid substances with slight modifications in the sensor design and the machine learning algorithms. The proposed sensor has the potential to find applications in health monitoring, automobile, food, and chemical industries, to name a few.

REFERENCES

1. Li, M., H.-L. Yang, X.-W. Hou, Y. Tian, and D.-Y. Hou, "Perfect metamaterial absorber with dual bands," *Progress In Electromagnetics Research*, Vol. 108, 37–49, 2010.
2. Rahimi, M., F. B. Zarrabi, R. Ahmadian, Z. Mansouri, and A. Keshtkar, "Miniaturization of antenna for wireless application with difference metamaterial structures," *Progress In Electromagnetics Research*, Vol. 145, 19–29, 2014.
3. Sabah, C. and S. Uckun, "Multilayer system of Lorentz/Drude type metamaterials with dielectric slabs and its application to electromagnetic filters," *Progress In Electromagnetics Research*, Vol. 91, 349–364, 2009.
4. Si, L.-M. and X. Lv, "CPW-fed multi-band omni-directional planar microstrip antenna using composite metamaterial resonators for wireless communications," *Progress In Electromagnetics Research*, Vol. 83, 133–146, 2008.
5. Smith, D. R., "How to build a superlens," *Science*, Vol. 308, No. 5721, 502–503, Apr. 22, 2005.
6. Amiri, M., M. Abolhasan, N. Shariati, and J. Lipman, "Soil moisture remote sensing using SIW cavity based metamaterial perfect absorber," *Scientific Reports*, Vol. 11, No. 1, 1–17, 2021.
7. Omer, A. E., G. Shaker, S. Safavi-Naeini, H. Kokabi, G. Alquié, F. Deshours, and R. M. Shubair, "Low-cost portable microwave sensor for non-invasive monitoring of blood glucose level: Novel design utilizing a four-cell CSRR hexagonal configuration," *Scientific Reports*, Vol. 10, No. 1, 1–20, 2020.
8. Vafapour, Z., W. Troy, and A. Rashidi, "Colon cancer detection by designing and analytical evaluation of a water-based THz metamaterial perfect absorber," *IEEE Sensors Journal*, Vol. 21, No. 17, 19307–19313, Jun. 9, 2021.
9. Tiwari, N. K., S. P. Singh, and M. J. Akhtar, "Novel improved sensitivity planar microwave probe for adulteration detection in edible oils," *IEEE Microwave and Wireless Components Letters*, Vol. 29, No. 2, 164–166, Dec. 28, 2018.
10. Tümkaya, M. A., F. Dinçer, M. Karaaslan, and C. Sabah, "Sensitive metamaterial sensor for distinction of authentic and inauthentic fuel samples," *Journal of Electronic Materials*, Vol. 46, No. 8, 4955–4962, Aug. 2017.
11. Abdulkarim, Y. I., Ş. Dalgaç, F. O. Alkurt, F. F. Muhammadsharif, H. N. Awl, S. R. Saeed, O. Altıntaş, C. Li, M. Bakır, M. Karaaslan, and M. Ameen, "Utilization of a triple hexagonal split ring resonator (SRR) based metamaterial sensor for the improved detection of fuel adulteration," *Journal of Materials Science: Materials in Electronics*, Vol. 32, No. 19, 24258–24272, Oct. 2021.
12. Bakır, M., Ş. Dalgaç, M. Karaaslan, F. Karadağ, O. Akgol, E. Unal, T. Depci, and C. Sabah, "A comprehensive study on fuel adulteration sensing by using triple ring resonator type metamaterial," *Journal of the Electrochemical Society*, Vol. 166, No. 12, B1044, Aug. 2, 2019.
13. Zhang, Y., J. Zhao, J. Cao, and B. Mao, "Microwave metamaterial absorber for non-destructive sensing applications of grain," *Sensors*, Vol. 18, No. 6, 1912, 2018.
14. Benkhaoua, L., M. T. Benhabiles, S. Mouissat, and M. L.Riabi, "Miniaturized quasi-lumped resonator for dielectric characterization of liquid mixtures," *IEEE Sensors Journal*, Vol. 16, No. 6, 1603–1610, Dec. 1, 2015.

15. Chuma, E. L., Y. Iano, G. Fontgalland, and L. L. Roger, "Microwave sensor for liquid dielectric characterization based on metamaterial complementary split ring resonator," *IEEE Sensors Journal*, Vol. 18, No. 24, 9978–9983, Oct. 1, 2018.
16. Zhou, H., D. Hu, C. Yang, C. Chen, J. Ji, M. Chen, Y. Chen, Y. Yang, and X. Mu, "Multi-band sensing for dielectric property of chemicals using metamaterial integrated microfluidic sensor," *Scientific Reports*, Vol. 8, No. 1, 1–11, 2018.
17. Kim, H. K., D. Lee, and S. Lim, "A fluidically tunable metasurface absorber for flexible large-scale wireless ethanol sensor applications," *Sensors*, Vol. 16, No. 8, 1246, Aug. 2016.
18. Yoo, M., H. K. Kim, and S. Lim, "Electromagnetic-based ethanol chemical sensor using metamaterial absorber," *Sensors and Actuators B: Chemical*, Vol. 222, 173–180, Jan. 1, 2016.
19. Prakash D. and N. Gupta, "High sensitivity grooved CSRR based sensor for liquid chemical characterization," *IEEE Sensors Journal*, Aug. 19, 2022.
20. Ekmekci, E., U. Kose, A. Cinar, O. Ertan, and Z. Ekmekci, "The use of metamaterial type double-sided resonator structures in humidity and concentration sensing applications," *Sensors and Actuators A: Physical*, Vol. 297, 111559, Oct. 1, 2019.
21. Ekmekci, E. and G. Turhan-Sayan, "Multi-functional metamaterial sensor based on a broad-side coupled SRR topology with a multi-layer substrate," *Applied Physics A*, Vol. 110, No. 1, 189–197, 2013.
22. Prakash, D. and N. Gupta, "Applications of metamaterial sensors: Review," *International Journal of Microwave and Wireless Technologies*, 1–15, 2021.
23. Ballard, Z., C. Brown, A. M. Madni, and A. Ozcan, "Machine learning and computation-enabled intelligent sensor design," *Nature Machine Intelligence*, Vol. 3, No. 7, 556–565, Jul. 2021.
24. Gocen, C. and M. Palandoken, "Machine learning assisted novel microwave sensor design for dielectric parameter characterization of water-ethanol mixture," *IEEE Sensors Journal*, Vol. 22, No. 3, 2119–2127, Dec. 15, 2021.
25. Patel, S. K., J. Surve, J. Parmar, A. Natesan, and V. Katkar, "Graphene-based metasurface refractive index biosensor for hemoglobin detection: Machine learning assisted optimization," *IEEE Transactions on Nano Bioscience*, Aug. 26, 2022.
26. Patel, S. K., J. Parmar, and V. Katkar, "Ultra-broadband, wide-angle plus-shape slotted metamaterial solar absorber design with absorption forecasting using machine learning," *Scientific Reports*, Vol. 12, No. 1, 1–4, Jun. 17, 2022.
27. Prakash, D. and N. Gupta, "Metamaterial inspired soil moisture sensor using machine learning approach for accurate prediction," *2021 3rd International Conference on Advances in Computing, Communication Control and Networking (ICAC3N)*, 642–646, IEEE, Dec. 17, 2021.
28. Riad, M. M. and A. R. Eldamak, "Coplanar waveguide based sensor using paper superstrate for non-invasive sweat monitoring," *IEEE Access*, Vol. 8, 177757–177766, Sep. 28, 2020.
29. Ebrahimi, A., W. Withayachumnankul, S. Al-Sarawi, and D. Abbott, "High-sensitivity metamaterial-inspired sensor for microfluidic dielectric characterization," *IEEE Sensors Journal*, Vol. 14, No. 5, 1345–1351, Dec. 18, 2013.
30. Bao, J. Z., M. L. Swicord, and C. C. Davis, "Microwave dielectric characterization of binary mixtures of water, methanol, and ethanol," *The Journal of Chemical Physics*, Vol. 104, No. 12, 4441–4450, Mar. 22, 1996.
31. Pedregosa, F., G. Varoquaux, A. Gramfort, V. Michel, B. Thirion, O. Grisel, M. Blondel, P. Prettenhofer, R. Weiss, V. Dubourg, and J. Vanderplas, "Scikit-learn: Machine learning in Python," *The Journal of Machine Learning Research*, Vol. 12, 2825–2830, Nov. 1, 2011.
32. Hastie, T., R. Tibshirani, J. H. Friedman, and J. H. Friedman, *The Elements of Statistical Learning: Data Mining, Inference, and Prediction*, Springer, New York, Aug. 2009.
33. Müller, A. C. and S. Guido, *Introduction to Machine Learning with Python: A Guide for Data Scientists*, O'Reilly Media, Inc., Sep. 26, 2016.

34. Kazemi, N., M. Abdolrazzaghi, and P. Musilek, "Comparative analysis of machine learning techniques for temperature compensation in microwave sensors," *IEEE Transactions on Microwave Theory and Techniques*, Vol. 69, No. 9, 4223–4236, May 31, 2021.
35. Kazemi, N., N. Gholizadeh, and P. Musilek, "Selective microwave zeroth-order resonator sensor aided by machine learning," *Sensors*, Vol. 22, No. 14, 5362, Jan. 2022.
36. Yang, R., Y. Li, J. Zheng, J. Qiu, J. Song, F. Xu, and B. Qin, "A novel method for carbendazim high-sensitivity detection based on the combination of metamaterial sensor and machine learning," *Materials*, Vol. 15, No. 17, 6093, Jan. 2022.
37. Wu, W. J., W. S. Zhao, D. W. Wang, B. Yuan, and G. Wang, "Ultrahigh-sensitivity microwave microfluidic sensors based on modified complementary electric-LC and split-ring resonator structures," *IEEE Sensors Journal*, Vol. 21, No. 17, 18756–18763, Jun. 17, 2021.
38. Badura, M., P. Batog, A. Drzeniecka-Osiadacz, and P. Modzel, "Regression methods in the calibration of low-cost sensors for ambient particulate matter measurements," *SN Applied Sciences*, Vol. 1, Jun. 2019.
39. Reis, M. S. and P. M. Saraiva, "Integration of data uncertainty in linear regression and process optimization," *AIChE Journal*, Vol. 51, No. 11, 3007–3019, Nov. 2005.
40. Moon, G., J. R. Choi, C. Lee, Y. Oh, K. H. Kim, and D. Kim, "Machine learning-based design of meta-plasmonic biosensors with negative index 0 metamaterials," *Biosensors and Bioelectronics*, Vol. 164, 112335, Sep. 15, 2020.